Quantum Mechanical Calculation of Reaction Probabilities and Branching Ratios for the $O(^1D) + HD \rightarrow OH(OD) + D(H)$ Reaction on the $\tilde{X}^1A'$ and $1^1A''$ Adiabatic Potential Energy Surfaces†

Marlies Hankel and Gabriel G. Balint-Kurti*

School of Chemistry, The University of Bristol, Bristol BS8 1TS, U.K.

Stephen K. Gray

Chemistry Division, Argonne National Laboratory, Argonne, Illinois 60439

Received: October 13, 2000; In Final Form: December 15, 2000

The real wave packet method is used to calculate state-to-state reaction probabilities and branching ratios for the reaction $O(^1D) + HD \rightarrow OH(OD) + D(H)$ for zero total angular momentum. Calculations are performed on the adiabatic potential energy surfaces corresponding to the $\tilde{X}^1A'$ and $1^1A''$ electronic states. Vibrational state-to-state cross sections, product state distributions and branching ratios are estimated using a capture model and *J*-shifting methods. The results are compared with experiment and with results of quasi-classical trajectory calculations.

I. Introduction

Our ability to accurately predict reactive scattering cross sections for gas-phase reactions started in 1976 with the seminal work of Schatz and Kuppermann.[1,2] In the current paper we will use different methods, which however still owe much to this initial work, to investigate the O + HD reaction.

The reaction $O + H_2 \rightarrow OH + H$, and its isotopic variants, has received considerable experimental[3−19] and theoretical[20−35] attention over the past decades. This interest has arisen from the fundamental importance of this reaction in combustion processes and in atmospheric chemistry.[3,4] The reaction of electronically excited oxygen $O(^1D)$ with H_2 and with its isotopomers D_2 and HD, is an important benchmark for the understanding of elementary reaction dynamics. The reaction

$$O(^1D) + H_2(^1\Sigma_g^+) \rightarrow OH(^2\Pi) + H(^2S) \qquad (1)$$

involves five potential energy surfaces (PES)[22−24,32,36−40] and at least the lowest three of them ($\tilde{X}^1A'$, $2^1A'$, $1^1A''$) may play a role in the reaction. For low collision energies, the reaction proceeds primarily on the lowest adiabatic PES 1A′. The ground-state PES which correlates with the ground electronic state of water is largely attractive and features a deep well for perpendicular geometries. Numerous theoretical studies[14,25,27,30,31] using quasi-classical trajectory (QCT) or quantum mechanical (QM) methods have been performed on the various different available ground-state adiabatic potential energy surface. Interest in the role of excited-state potential energy surfaces has arisen in the past few years as a result of several experiments.[11,13,15] These experiments, at higher collision energies, have been interpreted as pointing to the participation of excited states in the reaction. Recently there have been several experimental and theoretical studies aimed at investigating the participation of excited states in the $O + H_2$ reaction.[18,24,26,32,33,39]

For collinear OHH geometries the $O(^1D) + H_2(^1\Sigma_g^+)$ system splits into a $^1\Sigma^+$, a doubly degenerated $^1\Pi$ and doubly degenerated $^1\Delta$ component. The $^1\Delta$ state is purely repulsive and is omitted here. For collinear geometries the $^1\Sigma^+$ state gives rise to the lowest PES while the reagents approach. It correlates with the excited $A^2\Sigma^+$ state of the OH products and therefore cannot contribute to reaction. The $^1\Pi$ state connects adiabatically with the ground state of reactants and products and has a barrier of about 0.09 eV to reaction. For collinear geometries the $^1\Sigma^+$ and the $^1\Pi$ state feature a crossing. For bent geometries the $^1\Sigma^+$ state correlates with an A′ state and the $^1\Pi$ state splits into two components of A′ and A″ symmetry. The A′ state arising from the $^1\Sigma^+$ state mixes with the state of the same symmetry coming from the $^1\Pi$ state to give the 1A′ and 2A′ states. (Note that we will denote the $\tilde{X}^1A'$ surface as 1A′, the first excited state surface, $1^1A''$, as 1A″ and the second excited state, $2^1A'$, as 2A′.) These two states have a conical intersection at the location of the crossing of the $^1\Sigma^+$ and the $^1\Pi$ state. The lowest 1A′ surface has a deep well corresponding to the water molecule. The 1A″ surface has a collinear minimum energy reaction path corresponding to the collinear $^1\Pi$ state surface.

A few years ago Ho, Schatz and co-workers published an analytic potential energy surfaces for both the 1A′,[22] and 1A″,[23] states of the system. These surfaces were fitted to analytic forms using the reproducing kernel Hilbert space (RKHS) theory[22] and are known as the RKHS, or alternatively K, surfaces. More recently Dobbyn and Knowles produced a set of potentials that describe the lowest three states, 1A′, 1A″, and 2A′, and the couplings between them, thereafter denoted as the DK surfaces.[38,40,41] Both sets of surfaces, K and DK, were based on accurate ab initio multireference configuration interaction (CI) calculations with the difference that for the DK surface a slightly larger basis set was used. The RKHS method, which is used to fit an analytic form to the K surface, is guaranteed to pass exactly through all the ab initio computed points. The DK surface, on the other hand, is fitted to an analytic form using a method based on minimizing the square of the deviation between

† Part of the special issue "Aron Kupperman Festschrift."

* To whom correspondence should be addressed. Email: Gabriel.Balint-Kurti@Bristol.ac.uk.

10.1021/jp003772q CCC: $20.00
Published on Web 02/17/2001

the ab initio and the analytical potentials. This latter method inevitably introduces some additional errors. The most extensive theoretical studies of O + HD dynamics have been performed employing the K surface[22,23,30,35,42,43] but recently Aoiz et al.[44] carried out a thorough QCT study of the reaction dynamics on the 1A′, 1A″, and 2A′ DK surfaces. In the present work, a time-dependent method is used to calculate the branching ratio, reaction probabilities and product state distributions for the reaction O + HD → OD(OH) + H(D) on the 1A′ and 1A″ DK surfaces. Cross sections are then estimated using capture[31] and *J*-shifting[45] models.

The reaction can proceed through two different basic mechanisms, insertion and abstraction. In the insertion mechanism the oxygen atom inserts itself into the H−H bond to form an intermediate water complex. In the direct, or abstraction, mechanism the oxygen collides in a collinear configuration with the H−D and abstracts an H or D atom. The 1A′ PES favors the insertion mechanism and has no barrier for the C_{2v} approach. The lowest excited surface 1A″ favors the collinear approach and has a relatively low barrier, of about 0.1 eV, to reaction. Therefore, if only the ground state surface is considered as in most theoretical studies, the reaction proceeds mainly through the insertion mechanism. There have been various theoretical studies and several versions of the ground state adiabatic surface are available.[20,22,36,38] With increasing energy it is possible to overcome the barrier in the collinear geometry on the 1A″ surface and abstraction is expected to play a greater role. The dynamics on the 1A″ surface is therefore expected to be very different from that on the 1A′ surface and this should be reflected in the product state distributions. The abstraction mechanism is associated with an inverted vibrational distribution and a cold rotational distribution for the scattered product fragment OH(OD),[43,44] while the insertion mechanism is expected to lead to high rotational excitation and a monotonic decay in the population of the product vibrational states.

The next excited adiabatic PES, the 2A′, correlates with the ground state of the reactants but not with the ground state of the products and therefore can only contribute to reaction by nonadiabatic transitions. The barrier height on the 1A″ and 2A′ is the same in collinear geometry and these two excited states are not expected to play a significant role in the reaction for collision energies below 0.1 eV. Nonadiabatic transitions from the 2A′ to the 1A′ surface (and vice-versa) are facilitated by a conical intersection after the barrier on the collinear 2A′ surface.[39,44] The dynamics on the 1A″ surface can couple to that on the other surfaces through coriolis coupling. This effect has been studied by Drukker and Schatz,[32] who conclude that it makes a significant contribution. This coupling has not been included in the present study.

Hsu et al.[11] measured the reaction cross section for O + HD considering a collision energy range from 0.6 kcal/mol to nearly 6 kcal/mol (0.026 eV to 0.26 eV collision energy). They found that the reactive cross section for both product channels decreases for low energies and then starts to increase for collision energies greater than 0.1 eV. This was interpreted as an indication that the excited states contribute to reaction above 0.1 eV. Schatz et al.[23] performed QCT calculations on the 1A′ K and the 1A″ K surface considering the same energy range. Their summed cross sections [1A′ + 2(1A″)] also showed the rise at 0.1 eV but their calculated increase was less pronounced than that obtained in the experiment.

One of the important measurements is the isotopic branching ratio, OD/OH, of the two possible product channels OD + H and OH + D. For the F + HD system this problem has been elegantly analyzed by Johnston et al.[46] They conclude that, for this collinearly dominated reaction, there are conflicting dynamical and kinematic factors. The position of the center of mass of the HD reactant causes the cone of acceptance for the production of DF to be larger than that for the production of HF, but the dynamics leads to a sharp increase of the probability of forming HF relative to DF with increasing HD rotational quantum number. This last effect is stated to be dependent on the potential energy surface which is collinearly dominated as is that for the 1A″ surface. In the present case the favored product, OH or OD, arising from the abstraction mechanism is likely to be dependent on the details of the potential energy surface and of the rotational state of the reactants. When the insertion mechanism is dominant, the hydrogen leaves the newly formed complex with higher probability due to its lighter mass and greater velocity. In this case, one would expect a branching ratio greater than unity. Both experimental measurements and theoretical studies in fact predict a OD/OH branching ratio greater than unity.[44]

In section IIA the real wave packet method used in this work is described. In the section IIB the two approximation methods used to estimate the cross sections are outlined. The results are discussed in section III and conclusions are given in section IV.

II. Method

A. Dynamics. The real wave packet approach of Gray and Balint-Kurti[47] is used to calculate state-to-state reaction probabilities for zero total angular momentum. Wave packet methods yield results over a wide range of energies and for all populated product quantum states. The propagation of the wave packet is carried out in terms of Jacobi coordinates. To distinguish reactant and product Jacobi coordinates for a reaction A + BC → AB + C the latter are denoted with primes. The reactant coordinates are denoted by R, r, and γ, where R is the atom−diatom distance from A to the center of mass of BC, r is the BC internuclear distance, and γ is the Jacobi angle. In product coordinates, R' represents the scattering distance from C to the center of mass of AB, r' is the AB internuclear distance, and γ' the corresponding Jacobi angle. To obtain product quantum state resolved results the wave packet has to be analyzed in the product channel. The propagation is therefore carried out directly in product coordinates.

An alternative method for performing this type of calculation has been proposed[48−50] and used in particular in the work of Dai.[29] In this method the analysis is performed by calculating a time-dependent correlation function, rather than by collecting a set of time-dependent coefficients along an analysis line.[47,51,52] The advantages of this method are that reactant rather than product coordinates may be used to carry out the propagation, even when product quantum state distributions are desired. The disadvantage is that it is more difficult to confine the product state analysis to the asymptote of the product channel, as a finite sized product wave packet is used as part of the analysis procedure. In general terms the basis sets and number of grid points needed for the calculations are similar in both approaches.

The wave packet and the potential are represented by their values on a grid where the R' and r' grids are taken to be evenly spaced. The angular part of the wave packet is represented using a discrete variable representation (DVR),[53,54] which is based on Gauss−Legendre quadrature points. The potential matrix is diagonal in this representation, the evaluation of the rotational kinetic energy term involves a matrix multiplication and the kinetic energy terms associated with R' and r' are evaluated

using fast Fourier transforms.[51,55] The initial wave packet is set up in reactant coordinates, centered around an A−BC distance, $R = R_0$, and is then transformed to product coordinates, to carry out the propagation. The wave packet has to be analyzed at an appropriate large scattering distance, $R' = R'_\infty$, in the asymptotic region of the product channel. This makes the problem more difficult as the grid that is used has to contain the region where the initial wave packet is set up, the interaction region and the asymptotic region of the product channel where the wave packet is analyzed. Large grid sizes are therefore required. Another difficulty in the quantum dynamical treatment of $O(^1D) + HD$ is the large number of quantum states or equivalently grid points, needed to describe the motion in the well region.

To extract the necessary information from the wave packet, a cut is taken through it along the analysis line, $R' = R'_\infty$, at every iteration step. The resulting wave function is then projected onto the asymptotic diatomic product states, which results in an expansion of this wave function as a linear combination of the product state wave functions. This analysis method leads to a set of time-dependent coefficients (or more correctly iteration number dependent, see ref 47) which, when Fourier transformed, yield the ***S*** matrix elements, $S^J_{vj\rightarrow v'j'}(E)$, for every product state and over a wide range of energies, for which the wave packet has a reasonable amplitude.[47,51] Most wave packet propagations involve the propagation of an initial Gaussian wave packet in the scattering degree of freedom. For a Gaussian function the amplitude decreases as the energy deviates from the mean energy. An evenly distributed amplitude throughout the whole energy range should provide more accurate results in the energetic extremes. In the present work the Gaussian is multiplied by a *sinc* function, $\mathrm{sinc}\ x = (\sin x)/x$ and the initial wave packet used in the calculations is written as

$$\psi(R,r,\gamma,t{=}0) = g(R)\chi_{vj}(r)P_j(\cos\gamma) \tag{2}$$

$\chi_{vj}(r)$ represents the vibrational state wave function, $P_j(\cos\gamma)$ are the Legendre polynomials and

$$g(R) = N\mathrm{e}^{-ik_0(R-R_0)}\mathrm{e}^{-\beta(R-R_0)^2}\frac{\sin(\alpha(R-R_0))}{R-R_0} \tag{3}$$

$\exp(-ik_0(R-R_0))$ is a phase factor which gives the wave packet a relative kinetic energy toward the interaction region with $k_0 = \sqrt{2\mu E_{\mathrm{trans}}}$. N is a normalization factor. The Fourier transform of $g(R)$, the momentum distribution $\bar{g}(k)$, is given by

$$\bar{g}(k) = \frac{1}{2\pi}\int_0^\infty \mathrm{e}^{-ikR}g(R)\,\mathrm{d}R \tag{4}$$

which is needed in the calculation of the ***S*** matrix elements.[47] This choice of representation for the initial condition gives a smooth and relatively flat function for the momentum distribution, $\bar{g}(k)$, for suitable choices of β, E_{trans}, and α. It can therefore yield an almost constant amplitude for an energy range from $E_{\mathrm{min}} = ((k_0 - \alpha)^2)/2\mu$ to $E_{\mathrm{max}} = ((k_0 + \alpha)^2)/2\mu$.

The real wave packet approach[47] is advantageous for problems such as the present one where large grid and basis set sizes are required. Computer memory and computation time are significantly reduced because only the real part of the wave packet is employed. The wave packet evolves under a modified time-dependent Schrödinger equation

$$i\hbar\frac{\partial\psi(\mathbf{x},t)}{\partial t} = f(\hat{H})\psi(\mathbf{x},t) \tag{5}$$

where $\mathbf{x}$ denotes all coordinates, (R',r',γ'), and the Hamiltonian operator has been replaced by a function of itself

$$f(\hat{H}) = -\frac{\hbar}{\tau}\cos^{-1}(\hat{H}_s) \tag{6}$$

$\hat{H}_s = a_s\hat{H} + b_s$ is a scaled and shifted Hamiltonian operator such that its minimum and maximum eigenvalues lie between -1 and 1. This scaling is necessary to ensure the single valued mapping. If E_{min} and E_{max} are lower and upper bounds to the spectrum of $\hat{H}$, then $a_s = 2/\Delta E$ and $b_s = -1 - a_sE_{\mathrm{min}}$ with $\Delta E = E_{\mathrm{max}} - E_{\mathrm{min}}$. $\hat{H}_s$ is the same scaled Hamiltonian as that used by Tal-Ezer and Kosloff[56] in their Chebyshev expansion of the propagator. As $\hat{H}$ is represented using discrete radial grids and a finite set of angular functions E_{max} has a finite value. The propagation is more efficient if the energy range of the resulting Hamiltonian matrix is as small as possible and so a cutoff energy, V_{cut}, has been introduced and is applied to the potential to reduce the energy range. With this choice of the functional mapping of the Hamiltonian, the propagation of the wave packet is achieved by a Chebyshev iteration where each step requires only a single evaluation of the action of the Hamiltonian on a (real) vector. This approach shares many features with the work of Kouri and co-workers,[57,58] Mandelshtam and Taylor,[59,60] Kroes and Neuhauser,[61] and Chen and Guo.[62,63]

Let ψ be the representation of the wave packet at discrete grid points and let q denote the real part of the wave packet, $q = \mathrm{Re}\{\psi\}$, then the central equation of the real wave packet approach, propagating the real vector q according to Mandelshtam and Taylor's damped Chebyshev iterations,[59,60] is

$$q_{k+1} = \hat{A}\,(-\hat{A}q_{k-1} + 2\hat{H}_sq_k) \tag{7}$$

where k denotes the iteration step, $k = 1, \ldots, N$. Let q_0 be the real part and p_0 the imaginary part of the initial wave packet $\psi(R,r,\gamma,t = 0)$. The recursion relationship, eq (7), requires q_0 and q_1 to be initialized. In the present case the initial condition is complex and the initial step in the iteration process to evaluate q_1 is

$$q_1 = \hat{A}[\hat{H}_sq_0 - \sqrt{1-\hat{H}_s^2}p_0] \tag{8}$$

The effect of the square root is evaluated with a Chebyshev series expansion.[30] $\hat{A}$ is some appropriate operator which damps the wave packet amplitude as it approaches the grid edges. When finite grids are used the wave packet has to be absorbed to prevent it from reaching the end of the grid.

B. Capture Model and *J*-Shifting. The real wave packet method employed in this work, and the analysis of the wave packet in the product channel, yield state-to-state reaction probabilities over a wide range of energies. The calculations were performed for $J = 0$ only, whereas to calculate an integral cross section knowledge of the reaction probabilities for a large range of total angular momenta is required. For a relatively direct reaction, dominated by a barrier, standard *J*-shifting[45] may be used to estimate the reaction probabilities for total angular momentum values $J > 0$. If there is no significant barrier to reaction and the potential is attractive, *J*-shifting is not appropriate but a related approach, a capture model,[31] can be used. The capture model method is qualitatively like *J*-shifting. In *J*-shifting, there is a well defined bottleneck to reaction (with a structure that is assumed to be independent of *J*) that is used to determine the available energy in excess of the barrier for a given *J*. The transition state for the $1A''$ state is linear and the *J*-shifting formula for the reaction probability can be written as

$$P_r^J(E_{col}) = p(\epsilon = E_{col} - J(J+1)B) \quad (9)$$

where $J(J+1)B$ represents the rotational energy of the transition state with $B \approx 1.39$ cm^{-1} for OHD and $B \approx 1.77$ cm^{-1} for ODH. It is assumed that the reaction probability is a universal function, $p(\epsilon)$, of $\epsilon = E_{col} - J(J+1)B$ and this function therefore can be obtained from the $J = 0$ data. In the capture model method the bottleneck is determined by the centrifugal potential associated with each J. The effective potentials exhibit centrifugal barriers which differ for different J-values and are assumed to replace the barriers in the J-shifting. With V^J being the centrifugal barrier for a given J the formula for the capture model can be written as

$$P_r^J(E_{col}) = p_c(\epsilon = E_{col} - V^J) \quad (10)$$

Most of the details of the J-shifting and capture model method are well described elsewhere.[31,39,45] To calculate reactive cross sections on the attractive and barrierless 1A′ surface the capture model method was used. The 1A″ surface has a collinear minimum energy reaction path with a barrier in the entrance channel and therefore the J-shifting method was employed to calculate reactive cross sections for this electronic state. We estimated product vibrational state resolved cross sections on the 1A′ and 1A″ surface for both product channels. If $\sigma_{v'}(E)$ denotes the estimated cross section into a specific final v' state, then we can define the product distribution to be $\sigma_{v'}(E)/\Sigma'_v\sigma_{v'}(E)$.

C. Calculation Details. All calculations reported here are for total angular momentum $J = 0$. They were carried out in product Jacobi coordinates using the 1A′ and 1A″ adiabatic potential energy surfaces of Dobbyn and Knowles.[38,40,41] These surfaces are based on large scale multireference configuration interaction calculations. The 1A′ DK surface has no barrier for the C_{2v} insertion and just a small barrier of 0.019 eV for the collinear approach. The well depth is 7.29 eV. The zero point energy of the reactants O + HD is 0.23 eV and the reaction is exothermic by about 1.95 eV.

In all calculations the wave packet was analyzed along an analysis line in the asymptotic region of the product channel. This analysis yields all the reactive probabilities $P_r(E,v',j')$ for all relevant product states. The total reaction probability is then the sum over all v' and j' of $P_r(E,v',j')$. For the reaction of O(^{1}D) with HD there are two possible product channels, OD + H and OH + D. For each channel a separate calculation was performed using two different sets of product Jacobi coordinates. For the OD + H channel R' is the distance from H to the center of mass of OD and r' the internuclear distance of OD. For the OH + D product channel R' represents the distance from D to the center of mass of OH and r' is the OH internuclear distance. Using these two sets of product Jacobi coordinates the two calculations yield the reaction probabilities for the production of OD(v',j') and OH(v',j') in the reaction and the total reaction probabilities for each channel $P_r^{OH}(E)$ and $P_r^{OD}(E)$. The total reaction probability for O + HD is then the sum $P_r(E) = P_r^{OD}(E) + P_r^{OH}(E)$

In the calculations 80 angular DVR grid points were used which is equivalent to using rotational basis functions up to $j' = 79$. Not all of these are open asymptotically, however, and the wave packet was analyzed in the asymptotic region of the product channel to extract probabilities for the production of OD and OH in the lowest 10 vibrational states and the lowest 49 rotational states.

In the present work a double exponential damping operator, corresponding to an exponential imaginary absorbing potential,[64,65] has been used. The explicit form of the damping operator in (7) was taken to be $A_R(R)A_r(r)$ with the absorption functions $A_x(x) = \exp[-c_{abs}\exp(-2(x_{max} - x_{abs})/(x - x_{abs}))]$ for $x > x_{abs}$ and $\hat{A} = 1$ otherwise, where $x = R'$ or r'. The parameter c_{abs} controls the absorption strength, x_{abs} where the absorption region begins and $(x_{max} - x_{abs})$ is the length of the absorption region.

TABLE 1: Grid and Initial Condition Details for the Calculations[a]

scattering coordinate (R') range/a_0	0−16
number of gird points in R'	191
internal coordinate (r') range/a_0	0.5−16.5
number of grid points in r',	191
number of angular grid points	80
absorption region length in R' (r')/a_0	5 (5)
absorption strength (c_{abs})	0.5
center of initial wave packet (R_0)/a_0	9
width of the wave packet, α	8.0
smoothing of the wave packet, β	0.5
initial translational energy, E_{trans}/eV	0.2
cutoff energy, V_{cut}/eV	10.88
Hamiltonian scaling parameter[b] a_s/a_0	0.7592
Hamiltonian shift parameter[b] b_s/a_0	−0.7950

[a] All quantities are given in atomic units. [b] These parameters are computed automatically by the computer code. They differ for the two surfaces. The values quoted are for the 1A′ surface.

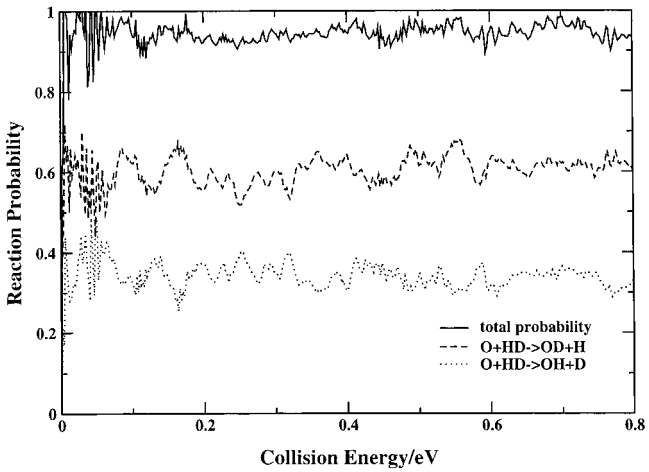

Figure 1. The reaction probability for the reactions O(^{1}D) + HD → OD + H (dashed line) and O(^{1}D) + HD → OH + D (dotted line) and the total reaction probability for O + HD (solid line) calculated on the 1A′ DK surface for $J = 0$.

All important parameters used in the calculations, including grid sizes, absorption parameters, and initial conditions are listed in Table 1. For both product channels and both surfaces the same parameters were used. Most of the calculations required about 50000 iterations steps to converge the results which corresponds to about 10 days computational time on a Silicon Graphics R12000 workstation. It would have been possible to use less dense grids, i.e., a smaller number of grid points, for the 1A″ surface due to the absence of the deep well in this case, but this possibility was not examined.

III. Results

A. Branching Ratio. Figure 1 shows the reaction probabilities ($J = 0$) calculated on the 1A′ surface for the two product channels, OH + D (dotted line) and OD + H (dashed line) and the total reaction probability for O + HD which is the sum of the two former (solid line). The total reaction probability is very high over the whole energy range and almost flat. In the low

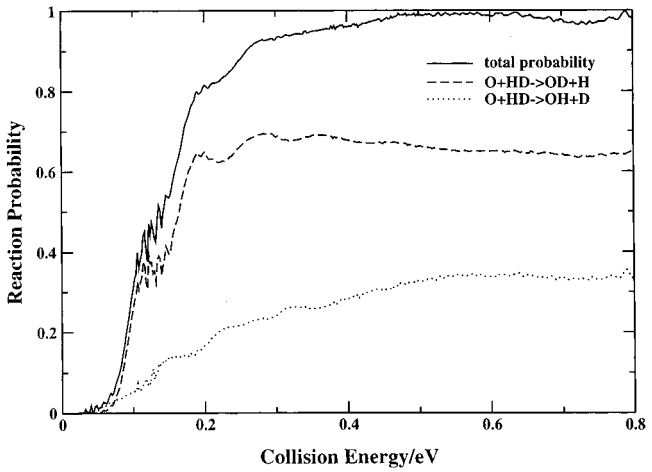

Figure 2. The reaction probability for the reactions $O(^1D) + HD \rightarrow OD + H$ (dashed line) and $O(^1D) + HD \rightarrow OH + D$ (dotted line) and the total reaction probability for O + HD (solid line) calculated on the 1A″ DK surface for $J = 0$.

collision energy region, from 0.0 to 0.07 eV, there are clearly some problems with the reactive probabilities predicted by our calculations. These problems mirror ones which have been observed at low collision energies for the $O + H_2$ system[28,29,34] and have been discussed in detail in ref 34. Figure 1 shows that the production of OD is preferred over the production of OH for all energies. One interesting feature of the structure of the probabilities for the two product channels is that when one of the channels has a maximum in its reaction probability the other one has a minimum. On one hand, as these are $J = 0$ only calculations, the fine structure in the total reaction probability and some of the structure of the reaction probabilities for the two different product channels will be smoothed out when higher *J*-values are included in the calculations. On the other hand, the complementary structure of the two product channel probabilities might be a real feature of the reaction on the ground-state surface. Figure 2 shows the $J = 0$ reaction probabilities computed for scattering on the 1A″ surface. This surface has a barrier of about 0.1 eV so there is a definite collision energy threshold to the reaction. It is clear again that the OD channel is preferred on this surface as well.

Figure 3 shows the branching ratio OD/OH for $J = 0$ (solid line) for reaction on the 1A′ and 1A″ surfaces over a collision energy range from 0 to 0.8 eV calculated from the reaction probabilities shown in Figures 1 and 2. The dashed line in Figure 3 represents the OD/OH ratio obtained from the cross sections estimated using the capture model for Figure 3a and using the *J*-shifting method for Figure 3b.[31] In Figure 3a the $J = 0$ ratio oscillates strongly with energy as a result of the oscillations of the individual probabilities of the two product channels with energy (see Figure 1). The ratio obtained from the capture model oscillates much less, increasing gently with energy from 1.6 to 1.8 over the energy interval shown. The average branching ratio of the $J = 0$ results, averaged over the energy range in Figure 3a, is estimated to be about 1.8 and the average branching ratio estimated from the approximate capture model cross sections is 1.71. Figure 3b shows the branching ratios obtained from scattering on the 1A″ surface. This ratio falls from values of about 6 to about 2.0 over the energy range examined.

Table 2 lists the experimentally measured branching ratios for two different collision energies, 2.4 and 3.4 kcal/mol, and also lists the corresponding values for $J = 0$ and those estimated from the capture model cross sections from the present work

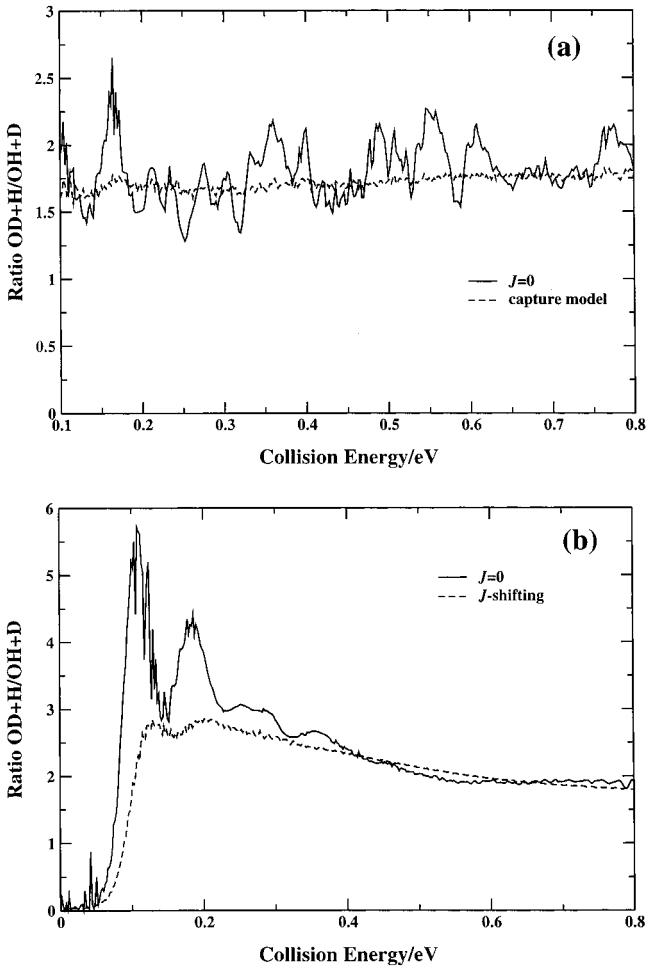

Figure 3. Branching ratio OD + H/OH + D over the collision energy range from 0.07 to 0.8 eV for $J = 0$ (solid line) and the result from the capture model (dashed line) calculated (a) on the 1A′ DK surface and (b) on the 1A″ DK surface.

TABLE 2: Branching Ratios Estimated from Experimental Measurements at Two Different Collision Energies[a] and the Corresponding Results from the Present Work for $J = 0$ and Using the Capture Model Employing the 1A′ DK Surface

2.4 kcal/mol	1.30 ± 0.1	LIF[66]
	1.13 ± 0.08	LIF[67]
	1.5 ± 0.2	REMPI[66]
	1.33 ± 0.07	VUV−RF[68]
	1.8	this work, $J = 0$
	1.69	this work, capture model
3.4 kcal/mol	1.35 ± 0.2	LIF[69]
	1.4 ± 0.2	REMPI[66]
	1.6	this work, $J = 0$
	1.7	this work, capture model

[a] These collision energies correspond to total energies of 0.33 and 0.37 eV.

on the 1A′ surface. The $J = 0$ ratios were calculated by averaging over an energy window of 0.01 eV. For the lower energy (~0.33 eV total energy) the ratio calculated in the present work is about 1.8 for $J = 0$ and 1.69 using the capture model. The ratios estimated from the experiment are all in the range of 1.1−1.5. For the higher collision energy (~0.37 eV total energy) the quantum dynamics results for $J = 0$ agree better with the experimental results and fall within the error bars of one of the experimental results at this energy. For both energies the branching ratio calculated in this work for $J = 0$ and the

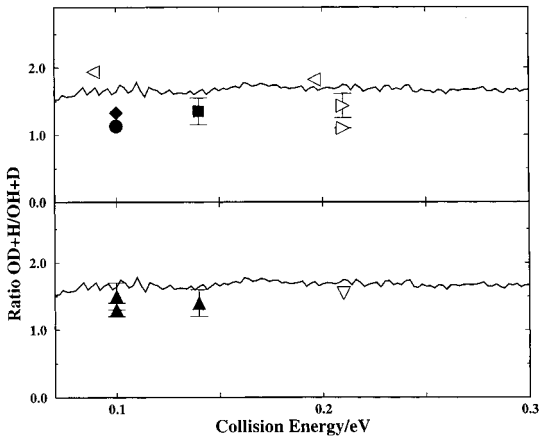

Figure 4. Branching ratio OD + H/OH + D: (1) calculated on the 1A′ DK surface in the present work using the capture model (solid line); (2) measured experimentally, ◆,[68] ●,[67] ▲,[66] and ■,[69] and (3) calculated using QCT methods employing different versions of the 1A′ surface, ▽[22] (K surface), left-pointing triangle[44] (DK surface), and right-pointing triangle[21] (SL1 and MC surface).

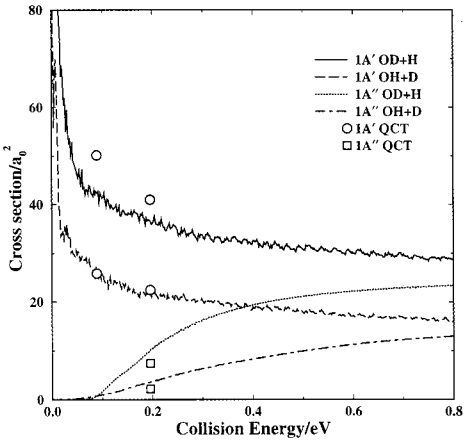

Figure 5. Integral cross sections for OD + H and OH + D vs collision energy in units of eV for the 1A′ (solid line for OD and dashed line for OH) and the 1A″ (dotted line for OD and dotted-dashed line for OH) DK surfaces calculated using the capture model (1A′) and *J*-shifting (1A″) methods. Included in the picture are the results from QCT calculations performed on the same surfaces[44] (circles for 1A′ and squares for 1A″).

ratio obtained from the capture model cross sections on the 1A′ surface are higher than the ratios measured in the experiments. It should be noted however that the present work does not really address the sensitivity of the cross section to the initial rotational state of the HD reactant. In most of the experimental work at least the $j = 1$ state of HD is substantially populated. Taking proper account of this might significantly alter our results.

To give a better overview of the ratios obtained from experimental and theoretical studies on the 1A′ surface, Figure 4 shows the ratio from the capture model displayed over a smaller energy range than in Figure 3a. Included in Figure 4 are the experimental results listed in Table 2 as well as results from QCT calculations performed on different versions of the ground adiabatic surface. Figure 4 shows good agreement with the experimental results from Matsumi et al.[66] and reasonable agreement with the results from Ho et al.[22] calculated on the 1A′ K surface and the results from Aoiz et al.[44] calculated on the 1A′ DK surface. (Note that these QCT calculations used an HD rotational temperature of 50 K. This results in 19% of the HD molecules being in the $j = 1$ rotational state.) In general, for the energy range shown, all the results from experiments and QCT calculations, except the most recent QCT calculation by Aoiz et al.[44] performed on the same surface as in this work, are lower than the ratio obtained in this work on the adiabatic 1A′ surface.

The branching ratio on the 1A″ surface was also calculated (see Figure 3b). This surface favors an abstraction and is similar in this respect to the case of F + HD discussed by Johnston et al.[46] In this work the average ratio on the 1A″ surface was calculated as 2.31 for $J = 0$ and as 2.0 using the *J*-shifting method. Aoiz et al.[44] calculated the branching ratio on the 1A″ surface for a collision energy of 0.196 eV. They give a ratio of 3.43 and the ratio calculated in the present work for this energy is 3.9 ($J = 0$) and 2.8 (estimate from the *J*-shifting). The branching ratio on the 1A″ surface is even higher than the ratio on the ground-state surface. As discussed by Johnston et al.[46] this is likely to result principally from the larger acceptance cone for formation of the OD product as compared with OH.

B. Cross Sections. Figure 5 shows the reactive cross sections vs collision energy for OD + H and OH + D calculated on the 1A′ DK (solid and dashed line) and on the 1A″ DK (dotted and dashed dotted line) surface. The cross sections are estimated using capture or *J*-shifting models as described in section IIB. Estimated reaction probabilities for *J*-values up to $J = 66$ were used for both the 1A′ and 1A″ surfaces. The maximum *J*-values depend on the maximum energy for which cross sections are requested and are such that there are no further estimated contributions to the cross section for higher values of *J*. The cross section for both product channels on the 1A′ surface decreases rapidly. For higher energies the cross section becomes almost flat. The cross section for both products on the 1A″ surface show the typical behavior for a reaction with a barrier. The threshold is at about 0.1 eV and the cross sections at first increase nearly linearly and then more slowly at higher energies.

Included in the figure are the results from a recent QCT study (circles and squares) by Aoiz et al.,[44] also employing the DK surfaces. For the 1A′ surface, Aoiz et al. report cross sections based on HD reactants at a temperature of 50 K. They also note that rotational excitation of the HD reactant does not substantially alter the cross section. In contrast, the cross sections on the 1A″ surface are found to be sensitive to the initial rotational quantum number[46] and in this case we have compared with the cross sections for HD($j = 0$) given in Table 2 of ref 44. The cross section for OH, calculated on the 1A′ surface, is in very good agreement with the QCT results. The estimated cross section for OD is lower than the cross section obtained in the QCT calculations. For the excited 1A″ surface the QM calculations give larger cross sections than the QCT ones for both product channels. Schatz et al.[23] have calculated the same cross sections for a range of collision energies from 0.6 kcal/mol to 10 kcal/mol (0.026 eV to 0.43 eV) on the K surfaces. The present results agree with the general features of the cross sections reported by Schatz et al.,[23] but also for these QCT results the cross section for OD on the 1A′ surface is higher and the cross section for OD and OH on the 1A″ surface are lower than the cross sections calculated in the present work.

The adiabatic 1A′ cross section has been found to be roughly equal to the sum of the 1A′ and 2A′ coupled state cross section for energies below the barrier on the collinear $^1\Pi$ surface (0.1 eV).[39] For higher energies the cross section on the 2A′ surface is roughly equal to the 1A″ cross section. Because the O(^{1}D) + HD system has five asymptotically degenerate states, we may

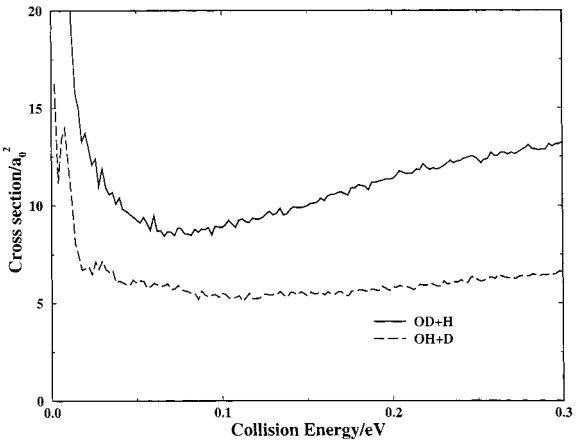

Figure 6. Estimated overall cross sections $\Sigma = {}^1/_5[\sigma_{1A'} + 2\sigma_{1A''}]$ for OD + H (solid line) and OH + D (dashed line) calculated from the results shown in Figure 5.

make a rough estimate of the full cross section for the reaction using the expression

$$\Sigma(E_{col}) = \frac{1}{5}[\sigma_{1A'} + 2\sigma_{1A''}] \quad (11)$$

This estimated cross section, for both channels, is shown in Figure 6. The estimates are likely to be upper bounds to the true cross sections as eq (11) does not take proper account of the diminution of the $\sigma_{1A'}$ cross section arising from electronically nonadiabatic transitions from the 1A′ to the 2A′ surface. Both cross sections are very large at low collision energies and show a steep decrease with increasing energy. The estimated cross sections of Figure 6 also show a minimum at the threshold of 0.1 eV followed by a gradual increase. For OD + H the minimum of the cross section is more pronounced than for OH + D. The increase at higher energies is similar to that found for the O + H_2 reaction[39] and arises from the contributions of the 1A″ state and estimated contribution of the 2A′ state to the overall cross section. Hsu et al.[11] measured the cross sections for OD + H and OH+D for a collision energy range from 0.6 to 6 kcal/mol (0.026 to 0.26 eV). The results from the present calculations agree well with these experimental results except for the OD + H/OH + D ratio. For energies below 0.1 eV, the reported experimental cross sections for OD + H and OH + D are nearly indistinguishable. Therefore, their measured ratio is nearly unity for low energies while the ratio obtained from the estimated cross sections shown in Figure 6 is about 1.6. Above the threshold the cross section for the OH + D products, reported by Hsu et al.,[11] remains nearly flat while that for OD + H increases which leads to a nearly linear increase of the ratio from 1.0 to 1.5 for energies above 0.1 eV. The results from the present work show a similar increase of the ratio above the threshold (i.e., above a collision energy of 0.1 eV). The experimental results also show that the minimum at 0.1 eV is more pronounced for OD + H than it is for OH + D, in agreement with the predictions of our calculations.

C. Product State Distributions. Figure 7 shows the vibrational distributions for OD and OH calculated on the 1A′ surface at the total energy of 0.4 eV. The figure shows the $J = 0$ results as well as the results from cross sections estimated using the capture model. While the $J = 0$ results show a lot of structure, most of it is smoothed out in the capture model results. The vibrational distribution for OD is inverted with a peak at $v' = 2$. The $J = 0$ results also show a second peak for $v' = 4$. For OH the most probable state for the capture model results is $v' = 0$. The $J = 0$ results show two peaks for $v' = 1$ and $v' = 3$. The OD distribution (for $J = 0$ and the capture model) is quite broad and vibrational states up to $v' = 7$ are populated. For OH the lower vibrational states are favored and the distribution ($J = 0$ and capture model) goes to zero for $v' = 5$. For energies greater than 0.4 eV, the distribution for OD always shows an inversion with the peak at $v' = 2$. With increasing energy the distributions get broader and states are populated up to $v' = 9$. For the OH distribution the most probable state remains $v' = 0$. For higher energies the distribution becomes completely flat for $v' = 1-3$ and then drops off. With increasing energy states up to $v' = 6$ are populated.

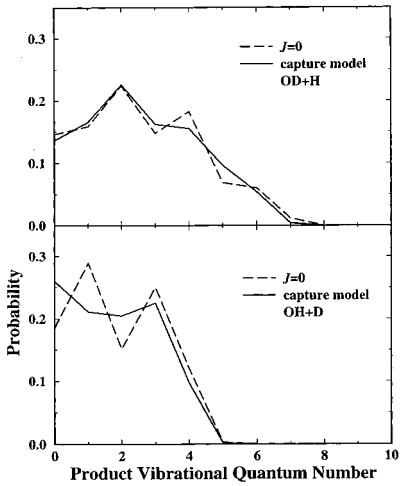

Figure 7. Product vibrational distributions of the products OD and OH obtained from the calculations performed on the ground-state surface 1A′ at $E_{tot} = 0.4$ eV. Shown are the distributions obtained using the $J = 0$ results (dashed line) and the results calculated using the capture model (solid line).

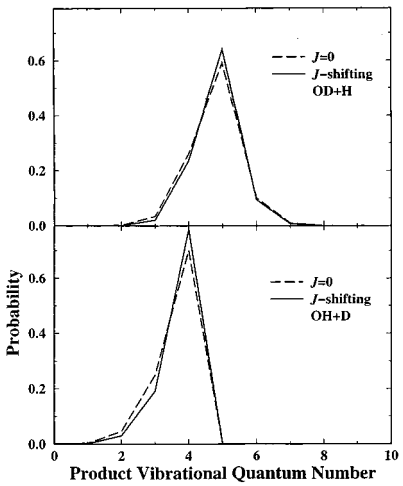

Figure 8. Product vibrational distributions of the products OD and OH obtained from the calculations performed on the excited surface 1A″ at $E_{tot} = 0.4$ eV. Shown are the distributions obtained using the $J = 0$ results (dashed line) and the results calculated using the *J*-shifting method (solid line).

Figure 8 shows the vibrational distributions calculated for the same energy on the 1A″ surface. These results show a complete different picture from the results on the 1A′ surface. The results for $J = 0$ are very similar to the results from the estimated cross sections using the *J*-shifting method for both OD and OH. For both products the vibrational distributions are highly inverted with a peak at $v' = 5$ for OD and $v' = 4$ for OH. This picture does not change much with increasing energy. For OD, the distributions have a very pronounced peak at $v' =$

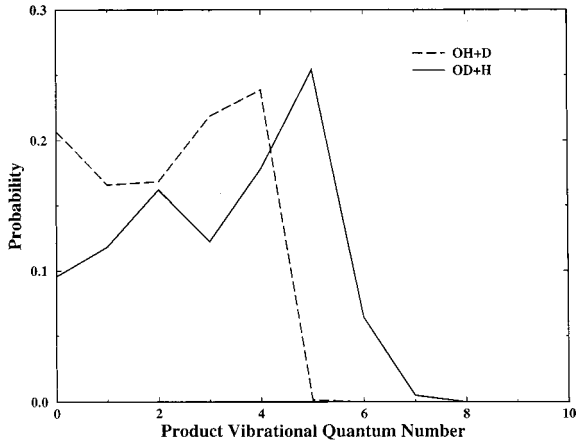

Figure 9. Estimated overall product vibrational distributions for OD (solid line) and OH (dashed line) at $E_{tot} = 0.4$ eV. The estimated cross sections were combined using equation 11 of the text.

5. Vibrational states from $v' = 3-7$ are populated while the population for $v' = 0-2$ is virtually zero. For OH the peak remains at $v' = 4$. With increasing energy states up to $v' = 5$ are populated and also the lower states get more and more populated. These results compare well to the results from QCT[43,44] calculations. In particular the QCT results from Hsu and Liu.[43] indicate that the OD product is favorably produced in the vibrational state $v' = 4-6$ and the product OH in the vibrational state $v' = 4$.

Figure 9 shows the overall product vibrational distributions for OD and OH calculated for a total energy of 0.4 eV (collision energy of 0.17 eV). These distributions were calculated from the estimated overall cross section obtained by applying equation (11) of the text. Both distributions are strongly inverted with a peak at $v' = 5$ for OD and $v' = 4$ for OH. These peaks result from the contribution of the 1A″ surface. For energies above the threshold of 0.1 eV the vibrational distribution for OD always shows the peak at $v' = 5$. For all energies there is basically no contribution from the first three vibrational states, $v' = 0-2$, arising from the excited state. With increasing energy, the states $v' = 3$ and $v' = 6$ become more and more populated while the population of the lowest three states gradually decreases. As the collision energy increases over 0.1 eV the population of OH($v' = 4$) steeply increases and then starts to decrease again. For high energies, the populations of $v' = 2-4$ are nearly the same and the OH vibrational distribution becomes almost flat for $v' = 2-4$. With increasing energy the states $v' = 1$ and $v' = 5$ become more and more populated with the population of $v' = 5$ arising exclusive from the contribution from the 1A″ surface.

Table 3 shows the QCT results of Ho et al.[22] calculated on the 1A′ K surface at a collision energy of 5 kcal/mol (≈0.44 eV total energy) and the results from the present work at the same energy for $J = 0$ calculated on the DK surface. For the vibrational distributions, the results obtained using the capture model are also shown in brackets. The table lists the vibrational distributions for OD and OH as well as the average rotational state, $\langle j' \rangle$, for each vibrational state and the average vibrational state, $\langle v' \rangle$. The uncertainties in the QCT calculations are ±0.01 for the vibrational population, ±0.03 for $\langle v' \rangle$ and ±1 for $\langle j' \rangle$ for every vibrational state. Table 3 shows good agreement for the OD/OH ratio and for the average product vibrational quantum number, $\langle v' \rangle$, for OH and OD between the present work and the QCT results. For OD both the QCT and the QM results show a similar trend in the vibrational distributions. Both show an inversion with a peak at $v' = 2$. The QM results for $J = 0$ also show a second peak at $v' = 0$ which does not appear in the capture model results. The QCT results show a steep decrease as one proceeds from $v' = 4$ to $v' = 5$. While the QM ($J = 0$) vibrational distribution for OD decreases rapidly going from $v' = 3$ to $v' = 4$, the capture model results show the same decrease going from $v' = 4$ to $v' = 5$ as the QCT results. For OH, the QCT and the QM vibrational distributions are in good agreement. Both show a continuous decay with $v' = 0$ as the most probable vibrational state. The QM ($J = 0$) show a slight peak for $v' = 4$ which is smoothed out in the capture model results. The capture model results for the vibrational distribution for OD and OH show very good agreement with the QCT results.

TABLE 3: QCT Results from Ho et al.[22] Calculated on the 1A′ K Surface for a Collision Energy of 5 kcal/mol (0.44 eV Total Energy) and the Results a the Same Energy Calculated in This Work on the 1A′ DK Surface[a]

QCT			this work		
OD/OH ratio		1.54	OD/OH ratio		1.7 (1.74)
			OD		
v′	P(v')	$\langle j' \rangle$	v′	P(v')	$\langle j' \rangle$
0	0.14	28	0	0.17 (0.14)	22
1	0.15	25	1	0.14 (0.17)	15
2	0.20	23	2	0.22 (0.23)	17
3	0.17	20	3	0.19 (0.17)	17
4	0.17	17	4	0.14 (0.17)	14
5	0.12	14	5	0.13 (0.11)	15
$\langle v' \rangle$	2.69		$\langle v' \rangle$	2.38 (2.36)	
			OH		
0	0.25	23	0	0.28 (0.25)	18
1	0.25	19	1	0.22 (0.22)	16
2	0.22	16	2	0.21 (0.21)	15
3	0.17	14	3	0.12 (0.21)	13
4	0.10	9	4	0.14 (0.10)	8
5	0.01	5	5	0.03 (0.01)	3
$\langle v' \rangle$	1.65		$\langle v' \rangle$	1.71 (1.72)	

[a] The results are for $J = 0$, and for the vibrational population, capture model results are also shown in brackets.

For the rotational distributions no capture model calculations were performed. The *J*-shifting and capture model methods are expected to be most accurate for the least resolved quantities. Therefore, we have concentrated on the vibrational state resolved cross sections and did not attempt to obtain v' and j' specific cross sections. The results shown for the average rotational state for every v' are $J = 0$ results and in general show that the QCT results give rise to more rotational excitation than the QM ones. One reason might be the differences between the 1A′ K and the 1A′ DK surfaces. As discussed in ref 34 for O + H_2, the 1A′ K surface leads to more rotational excitation than the 1A′ DK surface. For the vibrational distributions the agreement is better for the results obtained using the capture model. It is expected that the agreement for the rotational distribution will improve when higher *J*-values are also taken into account.

Butler et al.[9] measured the relative population of the vibrational states of OH and OD. They report the ratios of OH($v' = 1/v' = 0$) = 1.02 ± 0.2 and OD($v' = 1/v' = 0$) = 1.33 ± 0.2 and OD($v' = 2/v' = 0$) = 1.14 ± 0.2. The reagent translational energy associated with these measurements is somewhat ill defined but is probably a few kcal/mol. We calculated these ratios for collision energies of 2.4 and 3.4 kcal/mol from the vibrational distributions obtained in the present calculations on the 1A′ surface using the capture model. The calculated ratios are OH($v' = 1/v' = 0$) = 0.84 (0.76) and OD($v' = 1/v' = 0$) = 1.22 (1.20) and OD($v' = 2/v' = 0$) = 1.89 (1.62) for 2.4 kcal/mol (3.4 kcal/mol). The $v' = 1/v' = 0$ ratios for both products and energies calculated in this work agree

reasonably with the experimental results. The OD($v' = 2/v' = 0$) ratio is significantly higher than the one from the experiments and does not vary noticeably with energy within the range of the present calculations. As already discussed, the product vibrational state distribution predicted from dynamics on the 1A″ surface produces no significant population in either the $v' = 0$ to $v' = 2$ states, so the inclusion of this state in our results will not change any of the ratios discussed above.

IV. Conclusions

Integral cross sections, branching ratios, and product state distributions calculated using the real wave packet[47] approach have been presented for the reaction $O(^1D) + HD \rightarrow OH(OD) + D(H)$. The calculations were performed on the ground state adiabatic surface, 1A′, and the 1A″ adiabatic surface of Dobbyn and Knowles[38,40,41] for total angular momentum $J = 0$.

Cross sections have been estimated from the computed $J = 0$ reaction probabilities using the capture model[39] and *J*-shifting[45] approximations. We estimated cross sections for both product channels on both surfaces. The cross section for the OH + D channel on the 1A′ surface shows very good agreement with the results from a QCT calculation performed on the same surface.[44] The estimated cross section for the OD + H channel on the 1A′ surface is lower than that predicted by QCT calculations[23,44] and the cross sections on the 1A″ for both channels are higher.

An estimate is also made of the overall cross sections and product vibrational state distributions for the O + HD reaction which would be obtained if all three contributing electronic states had been properly taken into account. The overall cross sections show good agreement with experimental results.[11] The overall cross section for both channels decreases sharply for low energies and then starts to rise again above a collision energy of 0.1 eV. This increase arises from the contribution of the excited 1A″ and 2A′ states.

The OD/OH product ratios, based on dynamics just on the 1A′ surface, are found to be 15−20% higher than experimentally measured ratios (see Table 2). The theoretically determined dynamics on the 1A″ surface is found to yield even higher OD/OH ratios (see Figure 3b). Classical trajectory calculations on the same surface[44] give consistently higher OD/OH ratios than those estimated in the present quantum mechanical calculations. The available theoretical results therefore seem definitely to give a significantly higher OD/OH ratio than present experimental estimates.[11,66−68]

The vibrational distributions calculated using the 1A′ surface show an inversion for OD with a peak at $v' = 2$, while for OH $v' = 0$ is the most probable state. The vibrational distributions calculated on the 1A″ surface are very sharply peaked, with almost zero probability of $v' = 0,1$ occurring for OH and $v' = 0-2$ for OD. For OD the peak of the population occurs at $v' = 5$ and for OH it occurs at $v' = 4$. This agrees well with QCT calculations.[11,44]

The comparison between our quantum calculations and quasiclassical trajectory calculations is very good in all respects. Considering the uncertainty in the experimental results[9] our computed $v' = 1/v' = 0$ ratios are in good agreement with experiment. Our estimated OD($v' = 2/v' = 0$) ratio is a little high.

Acknowledgment. We thank the EPSRC for the provision of funds to purchase the computers on which this work was performed. M.H. thanks the University of Bristol for a postgraduate fellowship. S.K.G. was supported by the Office of Basic Energy Sciences, Division of Chemical Sciences, U.S. Department of Energy, under Contract W-31-109-ENG-38. We thank one of the referees for many helpful comments.

References and Notes

(1) Schatz, G. C.; Kuppermann, A. *J. Chem. Phys.* **1976**, *65*, 4624.
(2) Schatz, G. C.; Kuppermann, A. *J. Chem. Phys.* **1976**, *65*, 4642.
(3) Davidson, J. A.; Sadowski, C. M.; Schift, H. I.; Streit, G. E.; Howard, C. J.; Jennings, D. A.; Schmeltkopf, A. L. *J. Chem. Phys.* **1976**, *64*, 57.
(4) DeMore, W. B.; Sander, S. P.; Golden, D. M.; Hampson, R. F.; Kurylo, M. J.; Howard, C. J.; Ravishankara, A. R.; Kolb, C. E.; Molina, M., Chemical Kinetics and Photochemical Data for Use in Stratospheric Modeling. JPL Publication No. 94-26; Jet Propulsion Laboratory: Pasadena, CA, 1994.
(5) Butler, J. E.; MacDonald, R. G.; Donaldson, D. J.; Sloan, J. J. *Chem. Phys. Lett.* **1983**, *95*, 183.
(6) Luntz, A. C. *J. Chem. Phys.* **1980**, *73*, 1143.
(7) Aker, P. M.; Sloan, J. J. *J. Chem. Phys.* **1986**, *85*, 1412.
(8) Jursich, G. M.; Wiesenfeld, J. R. *Chem. Phys. Lett.* **1985**, *119*, 511.
(9) Butler, J. E.; Jursich, G. M.; Watson, I. A.; Wiesenfeld, J. R. *J. Chem. Phys.* **1986**, *84*, 5365.
(10) Smith, G. K.; Butler, J. E. *J. Chem. Phys.* **1980**, *73*, 2243.
(11) Hsu, Y.-T.; Wang, J.-H.; Liu, K. *J. Chem. Phys.* **1997**, *107*, 2351.
(12) Buss, R. J.; Casavecchia, P.; Hirooka, T.; Sibener, S. J.; Lee, Y. T. *Chem. Phys. Lett.* **1981**, *82*, 386.
(13) Che, D.-C.; Liu, K. *J. Chem. Phys.* **1995**, *103*, 5164.
(14) Alexander, A. J.; Aoiz, F. J.; Brouard, M.; Burak, I.; Fujimura, Y.; Short, J.; Simons, J. P. *Chem. Phys. Lett.* **1996**, *262*, 589.
(15) Hsu, Y.-T.; Liu, K. *J. Chem. Phys.* **1997**, *107*, 1664.
(16) Alexander, A. J.; Aoiz, F. J.; Brouard, M.; Short, J.; Simons, J. P. *Isr. J. Chem.* **1997**, *37*, 317.
(17) Alexander, A. J.; Aoiz, F. J.; Bañares, L.; Brouard, M.; Short, J.; Simons, J. P. *J. Phys. Chem.* **1997**, *101*, 7544.
(18) Alexander, A. J.; Aoiz, F. J.; Bañares, L.; Brouard, M.; Simons, J. P. *Phys. Chem. Chem. Phys.* **2000**, *2*, 571.
(19) Alexander, A. J.; Blunt, D. A.; Brouard, M.; Simons, J. P.; Aoiz, F. J.; Bañares, L.; Fujimura, Y.; Tsubouchi, M. *Faraday Discuss.* **1997**, *108*, 375.
(20) Schinke, R.; Lester, W. A. *J. Chem. Phys.* **1980**, *72*, 3754.
(21) Fitzcharles, M. S.; Schatz, G. C. *J. Phys. Chem.* **1986**, *90*, 3634.
(22) Ho, T.-S.; Hollebeek, T.; Rabitz, H.; Harding, L. B.; Schatz, G. C. *J. Chem. Phys.* **1996**, *105*, 10472.
(23) Schatz, G. C.; Papaioannou, A.; Pederson, L. A.; Harding, L. B.; Hollebeek, T.; Ho, T.-S.; Rabitz, H. *J. Chem. Phys.* **1997**, *107*, 2340.
(24) Schatz, G. C.; Pederson, L. A.; Kuntz, P. J. *Faraday Discuss.* **1997**, *108*, 357.
(25) Alexander, A. J.; Aoiz, F. J.; Bañares, L.; Brouard, M.; Herrero, V. J.; Simons, J. P. *Chem. Phys. Lett.* **1997**, *278*, 313.
(26) Alagia, M.; Balucani, N.; Cartechini, L.; Casavecchia, P.; van Kleef, E. H.; Volpi, G. G.; Kuntz, P. J.; Sloan, J. J. *J. Chem. Phys.* **1998**, *108*, 6698.
(27) Badenhoop, J. K.; Koizumi, H.; Schatz, G. C. *J. Chem. Phys.* **1989**, *91*, 142.
(28) Peng, T.; Zhang, D. H.; Zhang, J. Z. H.; Schinke, R. *Chem. Phys. Lett.* **1996**, *248*, 37.
(29) Dai, J. *J. Chem. Phys.* **1997**, *107*, 4934.
(30) Balint-Kurti, G. G.; Gonzalez, A. I.; Goldfield, E. M.; Gray, S. K. *Faraday Discuss.* **1998**, *110*, 169.
(31) Gray, S. K.; Goldfield, E. M.; Schatz, G. C.; Balint-Kurti, G. G. *Phys. Chem. Chem. Phys.* **1999**, *1*, 1141.
(32) Drukker, K.; Schatz, G. C. *J. Chem. Phys.* **1999**, *111*, 2451.
(33) Gray, S. K.; Petrongolo, C.; Drukker, K.; Schatz, G. C. *J. Phys. Chem.* **1999**, *103*, 9448.
(34) Hankel, M.; Balint-Kurti, G. G.; Gray, S. K. *J. Chem. Phys.* **2000**, *113*, 9658.
(35) Aoiz, F. J.; Bañares, L.; Herrero, V. J. *Chem. Phys. Lett.* **1999**, *310*, 277.
(36) Murrell, J. N.; Carter, S. *J. Phys. Chem.* **1984**, *88*, 4887.
(37) Durand, G.; Chapuisat, X. *Chem. Phys.* **1985**, *96*, 381.
(38) Dobbyn, A. J.; Knowles, P. J. *Faraday Discuss.* **1998**, *110*, 247.
(39) Gray, S. K.; Balint-Kurti, G. G.; Schatz, G. C.; Lin, J. J.; Liu, X.; Harich, S.; Yang, X. *J. Chem. Phys.* **2000**, *113*, 7330.
(40) Dobbyn, A. J.; Knowles, P. J. Unpublished data.
(41) Dobbyn, A. J.; Knowles, P. J. *Mol. Phys.* **1997**, *91*, 1107.
(42) Hsu, Y.-T.; Liu, K.; Pederson, L. A.; Schatz, G. C. *J. Chem. Phys.* **1999**, *111*, 7921.
(43) Hsu, Y.-T.; Liu, K.; Pederson, L. A.; Schatz, G. C. *J. Chem. Phys.* **1999**, *111*, 7931.
(44) Aoiz, F. J.; Bañares, L.; Brouard, M.; Castillo, J. F.; Herrero, V. J. *J. Chem. Phys.* **2000**, *113*, 5339.
(45) Bowman, J. M. *J. Phys. Chem.* **1991**, *95*, 4960.

(46) Johnston, G. W.; Kornweitz, H.; Schechter, I.; Persky, A.; Katz, B.; Bersohn, R.; Levine, R. D. *J. Chem. Phys.* **1991**, *94*, 2749.
(47) Gray, S. K.; Balint-Kurti, G. G. *J. Chem. Phys.* **1998**, *108*, 950.
(48) Judson, R. S.; Kouri, D. J.; Neuhauser, D.; Baer, M. *Phys. Rev. A* **1990**, *42*, 351.
(49) Tannor, D. J.; Weeks, D. E. *J. Chem. Phys.* **1993**, *98*, 3884.
(50) Dai, J.; Zhang, J. Z. H. *J. Phys. Chem.* **1996**, *100*, 6898.
(51) Balint-Kurti, G. G.; Dixon, R. N.; Marston, C. C. *Int. Rev. Phys. Chem.* **1992**, *11*, 317.
(52) Balint-Kurti, G. G.; Dixon, R. N.; Marston, C. C. *J. Chem. Soc., Faraday Trans.* **1990**, *86*, 1741.
(53) Lill, J. V.; Parker, G. A.; Light, J. C. *Chem. Phys. Lett.* **1982**, *89*, 483.
(54) Lill, J. V.; Parker, G. A.; Light, J. C. *J. Chem. Phys.* **1986**, *85*, 900.
(55) Kosloff, R. *J. Phys. Chem.* **1988**, *92*, 2087.
(56) Tal-Ezer, H.; Kosloff, R. *J. Chem. Phys.* **1984**, *81*, 3967.
(57) Huang, Y.; Kouri, D. J.; Hoffman, D. K. *J. Chem. Phys.* **1994**, *101*, 10493.
(58) Huang, Y.; Iyengar, S. S.; Kouri, D. J.; Hoffman, D. K. *J. Chem. Phys.* **1996**, *105*, 927.
(59) Mandelshtam, V. A.; Taylor, H. S. *J. Chem. Phys.* **1995**, *102*, 7390.
(60) Mandelshtam, V. A.; Taylor, H. S. *J. Chem. Phys.* **1995**, *103*, 2903.
(61) Kroes, G.-J.; Neuhauser, D. *J. Chem. Phys.* **1996**, *105*, 8690.
(62) Chen, R.; Guo, H. *J. Chem. Phys.* **1996**, *105*, 3569.
(63) Chen, R.; Guo, H. *Chem. Phys. Lett.* **1996**, *261*, 605.
(64) Vibók, Á.; Balint-Kurti, G. G. *J. Chem. Phys.* **1992**, *96*, 7615.
(65) Vibók, Á.; Balint-Kurti, G. G. *J. Phys. Chem.* **1992**, *96*, 8712.
(66) Matsumi, Y.; Tonokura, K.; Kawasaki, M.; Kim, H. L. *J. Phys. Chem.* **1992**, *96*, 10622.
(67) Tsukiyama, K.; Katz, B.; Bersohn, R. *J. Chem. Phys.* **1985**, *83*, 2889.
(68) Talukdar, R. K.; Ravishankara, A. R. *Chem. Phys. Lett.* **1996**, *253*, 177.
(69) Laurent, T.; Naik, P. D.; Volpp, H.-R.; Wolfrum, J.; Arusi-Parpar, T.; Bar, I.; Rosenwaks, S. *Chem. Phys. Lett.* **1995**, *236*, 343.